Check for updates

Energetics of a protein disorder–order transition in small molecule recognition†

Cesar Mendoza-Martinez,‡§ Michail Papadourakis,‡¶ Salomé Llabrés,‖ Arun A. Gupta,** Paul N. Barlow and Julien Michel ⓘ *

Many proteins recognise other proteins *via* mechanisms that involve the folding of intrinsically disordered regions upon complex formation. Here we investigate how the selectivity of a drug-like small molecule arises from its modulation of a protein disorder-to-order transition. Binding of the compound AM-7209 has been reported to confer order upon an intrinsically disordered 'lid' region of the oncoprotein MDM2. Calorimetric measurements revealed that truncation of the lid region of MDM2 increases the apparent dissociation constant of AM-7209 250-fold. By contrast, lid truncation has little effect on the binding of the ligand Nutlin-3a. Insights into these differential binding energetics were obtained *via* a complete thermodynamic analysis that featured adaptive absolute alchemical free energy of binding calculations with enhanced-sampling molecular dynamics simulations. The simulations reveal that in apo MDM2 the ordered lid state is energetically disfavoured. AM-7209, but not Nutlin-3a, shows a significant energetic preference for ordered lid conformations, thus shifting the balance towards ordering of the lid in the AM-7209/MDM2 complex. The methodology reported herein should facilitate broader targeting of intrinsically disordered regions in medicinal chemistry.

Introduction

Over 25% of proteomes in eukaryotes consist of proteins that lack a well-defined tertiary structure.[1,2] Nearly half of all proteins contain significant intrinsically disordered regions (IDRs), *i.e.* contiguous stretches of 20–50 amino acids that remain disordered in native conditions. IDRs are often key players in molecular recognition processes that underpin the affinity and selectivity of protein–protein interactions (PPIs).[3] A common scenario is that an IDR motif in a protein undergoes a disorder-to-order transition upon binding to another protein, leading to formation of a low-affinity high-selectivity complex.[4] Classical examples of disorder-to-order transitions include PPIs where one or both partner fold(s) into a well-structured protein upon binding.[5–7] However a growing number examples illustrate that one or both partner in a PPI may remain significantly disordered in the complex.[8–12]

Ample evidence points to the important roles of IDRs in the pathophysiology of diverse diseases such as cancers, diabetes or neurodegenerative disorders.[13] Consequently there is strong interest in developing therapeutic agents that interact with IDRs to modulate protein–protein interactions.[14,15] An appealing strategy would be to mimic Nature and identify small molecules that induce disorder-to-order transitions on binding to a target of interest.[16–18] To date examples of such small molecules have been largely discovered by serendipity. Consequently there is an unmet need for methodologies that facilitate the design of modulators of disorder-to-order transition in protein structures.[19–26]

With the view of advancing general understanding of small molecule–IDR interactions, the present report focuses on elucidating the energetics of a disorder-to-order transition mechanism observed upon binding of the small molecule AM-7209 to the N-terminal domain of the MDM2 protein (Fig. 1A and C). MDM2 is a negative regulator of the tumor suppressor p53.[27,28] The binding mechanism of p53 to MDM2 has been investigated previously *via* a variety of computational and experimental methods.[29–33] MDM2 is a validated drug target that has attracted vigorous medicinal chemistry efforts.[34–36] Several p53/MDM2 antagonists have entered clinical trials for diverse oncology indications.[37,38] AM-7209 is a lead molecule from the piperidinone family of MDM2 ligands.[39] Michelsen *et al.* used X-ray crystallography, NMR and biophysical experiments to demonstrate that piperidinone ligands order the N-terminal 'lid' IDR of MDM2 upon binding

EaStCHEM School of Chemistry, University of Edinburgh, David Brewster Road, Edinburgh, EH9 3FJ, UK. E-mail: mail@julienmichel.net

† Electronic supplementary information (ESI) available. See https://doi.org/10.1039/d2sc00028h

‡ These authors made equal contributions.

§ Present Address: R&D Department, TECSIQUIM S.A de C.V, Parque. Ind. Toluca 2000, 50200, Toluca de Lerdo, México.

¶ Present Address: Biomedical Research Foundation, Academy of Athens, 4 Soranou Ephessiou Street, 11527, Athens, Greece.

‖ Present Address: Department of Nutrition, Food Science and Gastronomy, Faculty of Pharmacy and Food Science, University of Barcelona, Prat de la Riba 171, 08921 Santa Coloma de Gramenet, Spain.

** Present Address: Department of Chemistry, University of Warwick, Coventry, CV4 7AL, UK.
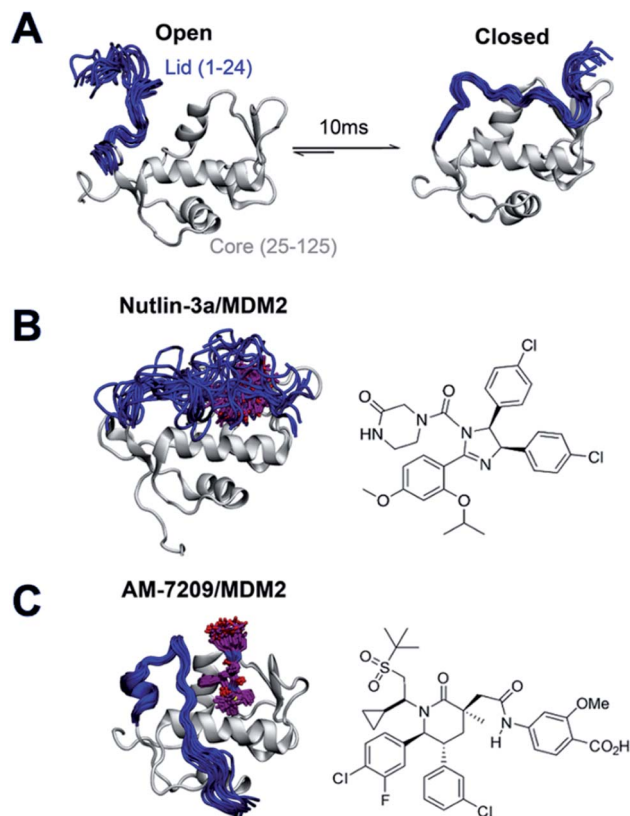
Fig. 1   Ligand-specific modulation of conformational preferences of the MDM2 N-terminal domain lid IDR. (A) In apo MDM2 the lid region is disordered and exchanges on a millisecond timescale between 'open' and 'closed' disordered conformational states that regulate access to the p53-binding site.[30,32] (B) Previous work from Bueren-Calabuig and Michel suggests the ligand Nutlin-3a binds MDM2 with the lid in 'closed' state broadly similar to that seen in apo.[31] (C) Binding of the MDM2 ligand AM-7209 orders the MDM2 lid region into a helix-turn-strand motif.[31,40] Representative snapshots of the lid conformations are taken from the simulations reported in this manuscript.

(Fig. 1C).[40] By contrast the p53/MDM2 antagonist Nutlin-3a binds to MDM2 without ordering the lid region (Fig. 1B).[40,41]

Currently it is not understood why piperidone ligands order the MDM2 lid IDR, whereas other ligands such as Nutlin-3a do not. Such knowledge would greatly facilitate the rational design of ligands targeting protein IDRs, and open new opportunities to modulate protein function with small molecules. Here we provide a rationale for the different binding mechanisms of AM-7209 and Nutlin-3a by combining calorimetric measurements with a novel method for performing absolute free energy of binding calculations, and with enhanced-sampling molecular dynamics (MD) simulations. The results pave the way for broader targeting of IDRs in structure-based drug design campaigns.

Results and discussion

Truncation of the MDM2 lid IDR modulates AM-7209 affinity by 250-fold

We prepared protein constructs for human MDM2 6-125 and MDM2 17-125 (Fig. S1 and S2,† referred to as MDM2-Lid and

MDM2-Lid/short from here on). These constructs were chosen to be similar to those used by Michelsen *et al.* for ITC measurements on Nutlin-3a and selected piperidone ligands.[40] Michelsen *et al.* showed that truncation of the first five residues of the N-terminal region of MDM2 has negligible effects on measured binding affinities, whereas truncation of the first sixteen residues significantly affects the binding affinity of piperidinone ligands only.[40] As measurements of the binding affinity of AM-7209 to a MDM2-Lid/short variant have not been reported we carried out ITC measurements to study the effect of lid truncation on Nutlin-3a and AM-7209 binding. Previous reports indicate that both compounds bind to MDM2 with a 1 : 1 stoichiometry.[39,41] The present experiments gave well behaved titrations with similar errors for all complexes (Fig. S3, S4 and Table S1†). In the case of Nutlin-3a lid truncation only weakly increases the apparent dissociation constant, by 1.2–2.3 fold (Fig. 2A), without significant changes in enthalpy or entropy of binding (Fig. 2B and C). These observations are in broad agreement with previous reports.[40] Our measurements
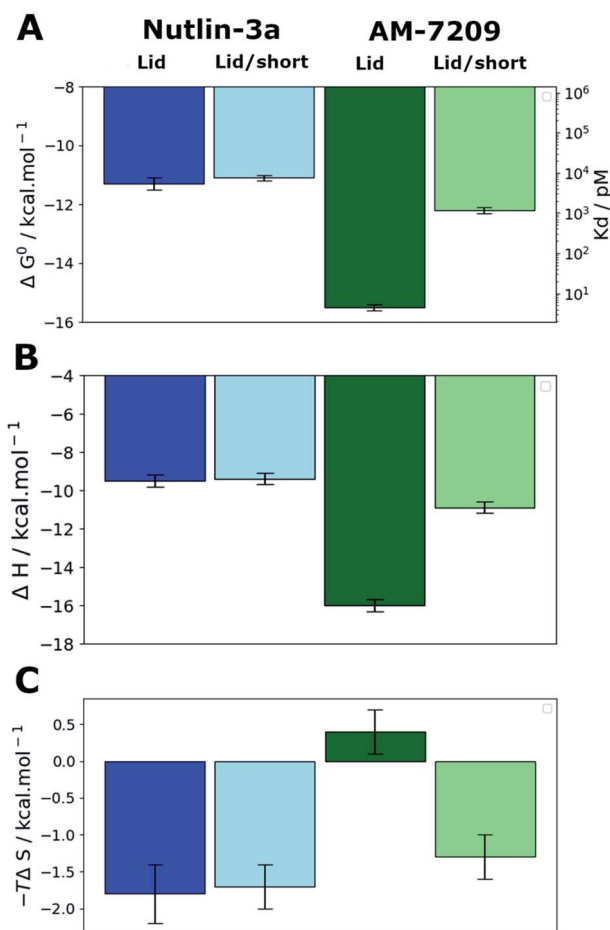

Fig. 2   MDM2 lid truncation has a differential effect on thermodynamic signatures of Nutlin-3 and AM-7209 binding. (A) Apparent standard Gibbs free energies of binding and dissociation constants measured by ITC experiments. (B) Enthalpies of binding. (C) Entropies of binding. Dark blue: Nutlin-3a/MDM2-Lid. Light blue: Nutlin-3a/MDM2-Lid/short. Dark green: AM-7209/MDM2-Lid. Light green: AM-7209/MDM2-Lid/short. Error bars denote ±1σ (n = 3).

reveal that AM-7209 is an extraordinarily potent ligand for MDM2-Lid, with an apparent K_d value of *ca.* 5 ± 1 pM (Fig. 2A). In the case of AM-7209, lid truncation causes a significant increase in the enthalpy of binding, and a decrease in the entropy of binding (Fig. 2B and C). Thus, changes in enthalpy favour binding of AM-7209 to MDM2-Lid over MDM2-Lid/short. This suggests that additional interactions between the MDM2 lid region and AM-7209 or the MDM2 core region are present in the AM-7209/MDM2-Lid complex in comparison with the AM-7209/MDM2-Lid/short complex. The lack of difference in enthalpies of binding of Nutlin-3a between the two MDM2 constructs suggest that AM-7209 induces a distinct conformational change in the MDM2 lid region over Nutlin-3a. As changes in entropy disfavour binding of AM-7209 to MDM2-Lid over MDM2-Lid/short, this suggests that such lid conformational change is associated with increased rigidity of the lid region in the AM-7209/MDM2-Lid complex over the Nutlin-3a/MDM2-Lid complex. The net effect of lid truncation in the case of AM-7209 binding to MDM2 is a remarkable 250-fold increase in apparent K_d.

Spontaneous ordering of the MDM2 lid is energetically disfavoured in apo MDM2

Clarification of the intrinsic energetic preferences of the MDM2 lid IDR was sought by using molecular dynamics (MD) simulation methodologies. Forcefield development for molecular dynamics simulations of IDPs is an active research area.[25,42] The choice of solvent model and protein forcefield greatly influences the conformational ensembles gathered from MD simulations.[43–45] For the specific case of protein IDRs simulations, forcefields that correctly describe both the intrinsically disordered regions and the folded regions of the protein are required.[25,46] There is no consensus yet on which is the best forcefield for IDRs as the accuracy of the predictions seem to depend on the studied protein. Here we used the amber99SB-ildn-nmr forcefield because it was shown to reproduce reasonably the behaviour of ordered motifs in proteins,[47] and the disordered N-terminal tail region of histone H3.[48] Previous studies with this forcefield have also given a reasonable description of the MDM2 lid IDR dynamics.[31–33]

Estimation of a free-energy surface for the lid region was carried out using a MD simulation-sampling protocol that combines accelerated molecular dynamics (aMD),[49] Umbrella Sampling (US),[50] and variational free-energy profile (vFEP) methodologies (see ESI text, Table S2 for protocol details and Fig. S5 for convergence estimates†).[51] This approach has been used in previous studies of MDM2 lid dynamics,[31,32] but ordered lid conformations could not be detected in the computed apo ensembles. Evaluation of the conformational energetics of the MDM2 lid IDR by use of a free energy surface requires finding a low-dimensionality projection that separates ordered and disordered lid conformations. This was achieved here by carrying
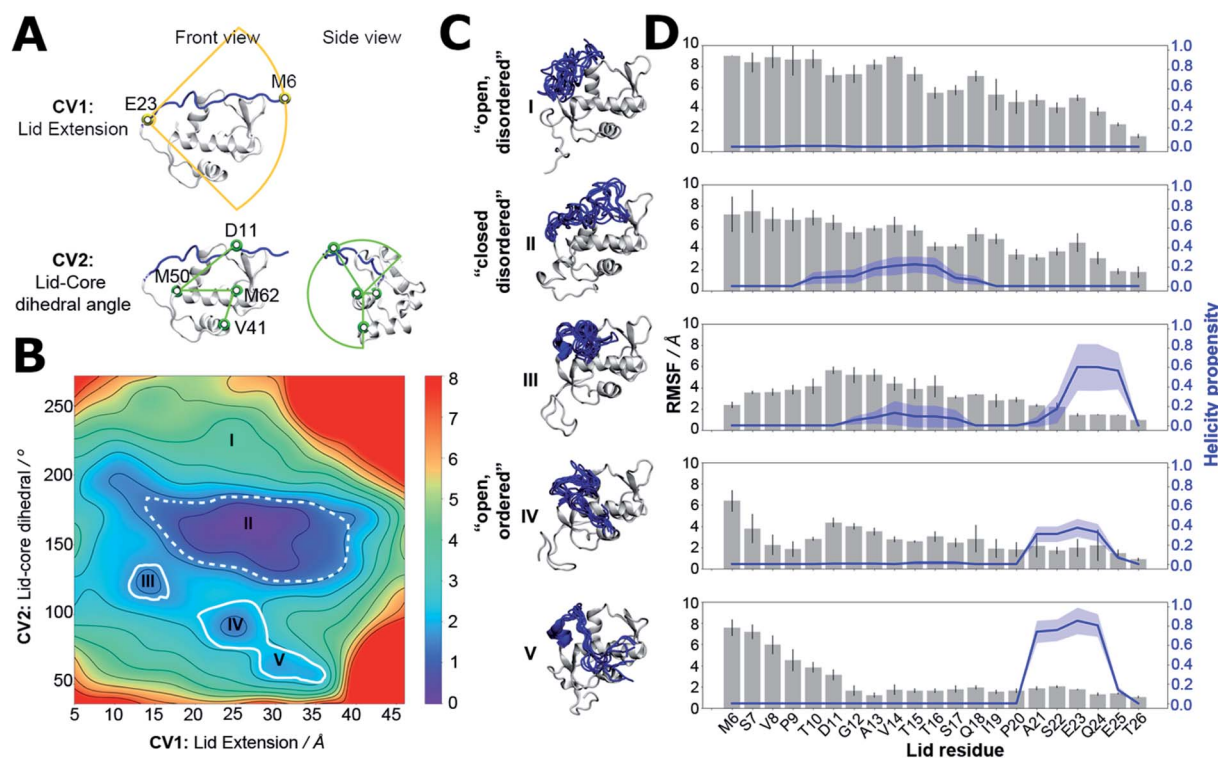

Fig. 3 The lid IDR predominantly adopts a closed and disordered macrostate in apo MDM2. (A) Collective variables used for aMD/US/vFEP calculations. (B) Free-energy surface of apo MDM2. Heatmap scale in kcal mol^{-1}. Contours used to estimate macrostate populations are shown with solid lines (open and ordered macrostate) or dashed lines (closed and disordered macrostate). (C) Representative snapshots from different macrostates highlighted in the free-energy surface are shown with the lid IDR highlighted in blue. (D) Structural properties of the lid in the distinct states highlighted in panels (B) and (C). Error bars denote $\pm 1\sigma$ from the first and last halves of the US simulations.

out independent aMD simulations on models of apo-MDM2, Nutlin-3a/MDM2 and AM-7209/MDM2, initiated with the lid IDR in distinct conformations observed in NMR and X-ray experiments. Snapshots sampled from the different aMD simulations were pooled and projected on different 2D and 3D collective variables drawn from geometric descriptors supported by the AMBER16 suite for follow up US simulations. To avoid excessively time-consuming Umbrella sampling calculations, we settled down on a 2D representation that monitors the end-to-end distance of the lid and the relative position of the lid with respect to the core region (Fig. 3A). Such representation was able to separate ordered lid conformations observed in the AM-7209 complex from other conformations seen during the aMD simulations. Analysis of the free-energy surface obtained after vFEP processing of the US trajectories indicates that in apo MDM2 the lid IDR adopts a major "closed and disordered" lid macrostate that accounts for *ca.* 75–80% of the lid's conformational ensemble (Table S3†). This macrostate is characterised by a diverse range of lid conformations that extend above helix α2 and the p53-binding site, with occasional formation of helical motifs in the middle of the IDR region (Fig. 3B–D). Formation of an "open and disordered" macrostate is energetically strongly disfavoured, and it accounts for less than 1% of the ensemble in

the present simulations (Fig. 3B–D). An "open and ordered" macrostate featuring comparatively lower positional fluctuations throughout the lid IDR and a helix-turn-strand motif, similar to that seen in X-ray structures of AM-7209/MDM2 complexes, accounts for *ca.* 6–8% of the ensemble (Fig. 3B and C). Such a low population may explain why it would have been difficult to observe directly the "open and ordered" lid macrostate in previous NMR experiments performed on apo MDM2.[30]

An adaptive sampling protocol enables efficient computation of binding energetics for MDM2 ligands

The free energy surface analysis indicates that the "open and ordered" lid macrostate is less stable than the "closed and disordered" macrostate by *ca.* 1.4 ± 0.2 kcal mol^{-1}. To clarify why such a macrostate is predominant in the AM-7209/MDM2 complex it is necessary to determine ligand-binding energetics to distinct lid macrostates. Alchemical absolute binding free-energy calculations (ABFE) may in principle be used for this purpose. Here we use a double decoupling methodology with orientational restraints (Fig. S8†) and standard state corrections to compute standard free energies of binding (Fig. S6 and ESI text†).[52–57]
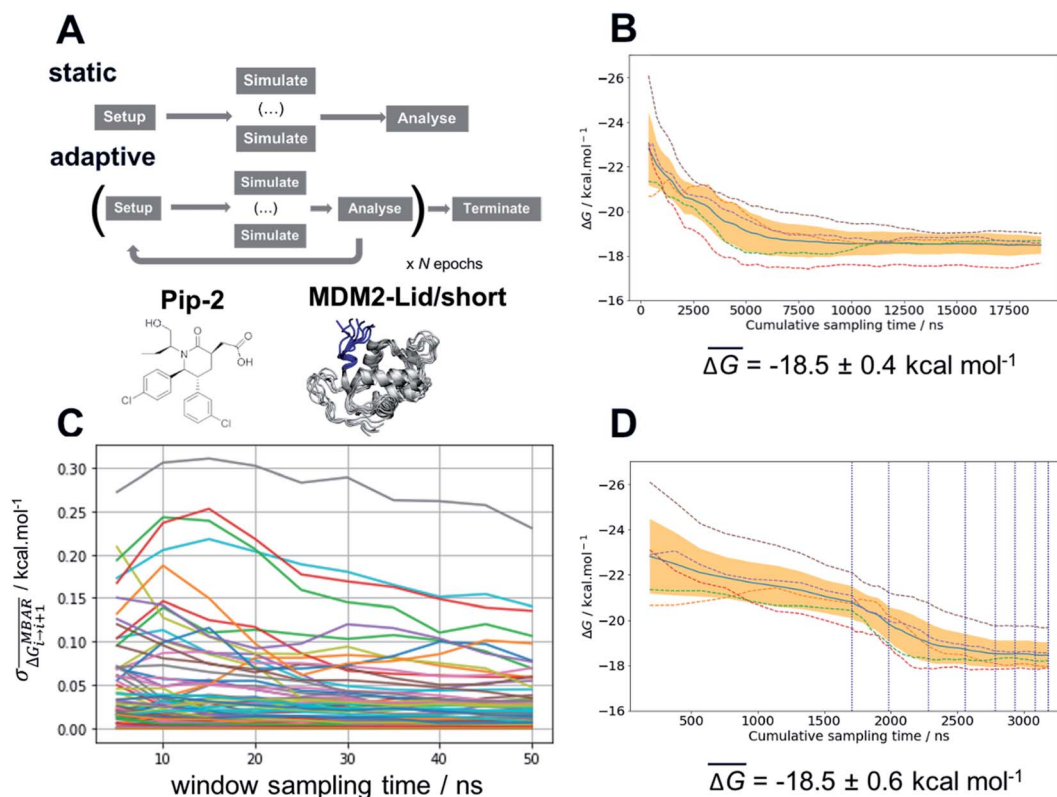

Fig. 4 Adaptive sampling of the λ-schedule significantly improves the efficiency of alchemical absolute binding free-energy calculations. (A) Schematic description of static and adaptive alchemical absolute binding free energy calculation protocols. (B) Convergence of computed binding free energies for Pip-2 in complex with MDM2-Lid/short with a static protocol. Dashed lines are for individual replicates ($n = 5$). The solid blue line denotes the mean of the five replicates and the orange shaded area denotes the 95% confidence interval on the mean of the five replicates. Standard-state corrections have not been applied. (C) Evolution of the standard deviation of the mean MBAR free-energy change ($n = 5$) over time for successive pairs of windows i, $i + 1$ across the λ-schedule. Data for each window pair plotted with a different colour for illustrative purposes only. (D) Convergence profile for free-energies of Pip-2 binding using an adaptive protocol and threshold, $\tau = 0.100$ kcal mol^{-1}. Vertical blue dotted lines denote successive epochs of the adaptive protocol. Other details similar to panel (B).

Achieving reasonable convergence of the computed binding free energies with ABFE methodologies remains very challenging for lead-like molecules bound to flexible protein regions. Here we addressed this issue by developing an adaptive sampling protocol that optimises resource allocation to produce free-energy of binding estimates at a fraction of the computing costs required for a standard protocol (Fig. 4A). The adaptive protocol was initially benchmarked on the structurally related but simpler ligand, Pip-2, in complex with MDM2-Lid/short. These calculations were carried out using the Amberff14SB forcefield as the amber99SB-ildn-nmr forcefield was not supported by our ABFE setup tool FESetup version 1.2. Reliable binding free-energy estimates could be obtained with a standard protocol where the same sampling time of 50 ns is allocated to each of the windows used to decouple the ligand in the bound and the free state (12 for decoupling electrostatic interactions, 26 for decoupling Lennard-Jones interactions in each bound/free stages, giving a total of 76 windows for the full λ-schedule). Five replicates are carried out to estimate a mean binding free energy and confidence interval, which amounts to a cumulative sampling time of 19 μs (Fig. 4B). Fig. 4C indicates that fluctuations in the mean free energy changes between successive windows are unevenly distributed along the λ-schedule. A few windows require significantly more sampling time to decrease statistical fluctuations to a level where the mean binding free energy estimate reaches a plateau. These windows correspond to stages of the λ-schedule where the

bound state ligand Lennard-Jones interactions are partially decoupled. Such states give noisy free energy changes unless long sampling time are used because diffusion of water molecules in the protein binding site is frustrated by the presence of the partially decoupled ligand.

To address this sampling difficulty whilst minimising use of computing resources we implement an adaptive sampling protocol. Quintuplicate simulations are carried out for a period of 5 ns (an "epoch") across a predefined λ-schedule. Once an epoch has completed, the free-energy change between neighbouring windows is estimated using the Multistate Bennett Acceptance Ratio method (MBAR).[58] Windows whose standard deviation of the mean free-energy change exceeds a threshold parameter, τ, are automatically carried forward to the next epoch. The protocol is iterated for a set number of epochs or until the standard deviation of all windows drops below τ. Thus, as the simulations progress, computing resources are automatically focussed on parts of the λ-schedule that require more effort to compute sufficiently precise free energy changes. Significant savings of compute resource may therefore be achieved by the early termination of sampling of well-behaved windows. Fig. 4D depicts a convergence profile for an adaptive sampling run with $\tau = 0.100$ kcal mol^{-1}. The threshold parameter τ must be chosen with care. A too low value yields little savings in computing time, a too high value may cause the simulations to terminate prematurely and yield a biased binding free energy estimate. Additional experiments
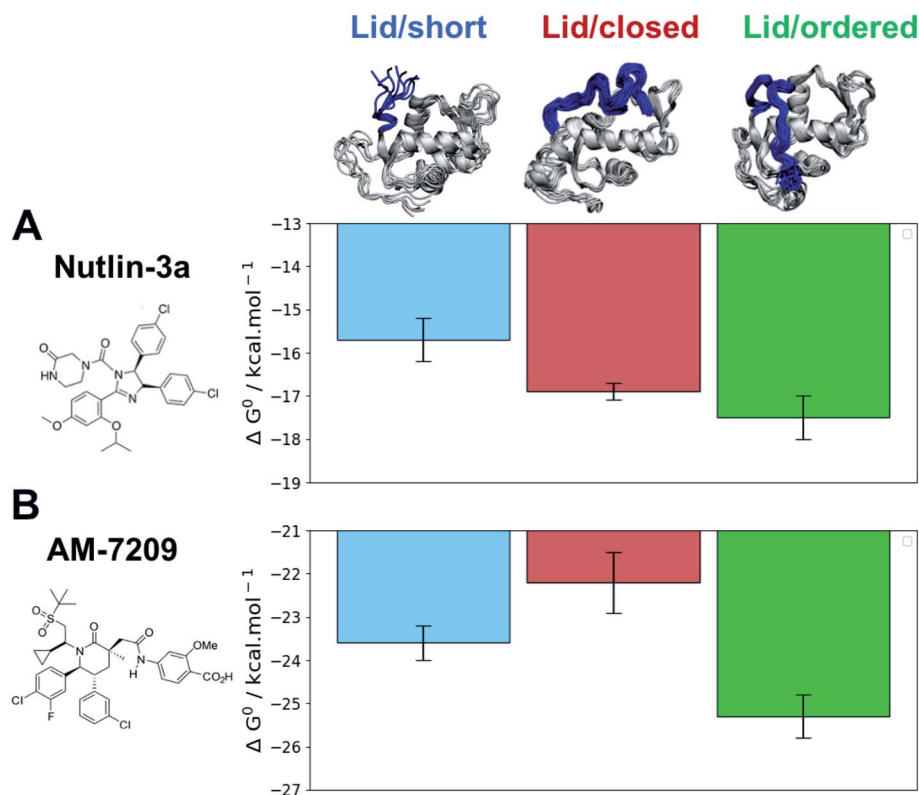

Fig. 5 Adaptive ABFE calculations reveal a marked preference of AM-7209 for the MDM2/Lid-closed state. (A) Computed standard free-energies of binding for Nutlin-3a. (B) Computed standard binding free-energies for AM-7209. Error bars denote $\pm 1\sigma$ ($n = 5$).

determined that $\tau = 0.100$ kcal mol^{-1} gives the best speed/accuracy trade-off for the present system (see ESI text and Fig. S7 for convergence plots†). Results statistically indistinguishable from the brute-force calculation are achieved with an almost six-fold decrease in computing resources requirement.

AM-7209 but not Nutlin-3a shows a marked preference for binding to ordered lid conformations

The efficiency gains observed with the adaptive sampling encouraged us to pursue the more challenging ABFE simulations of AM-7209 and Nutlin-3a in complex with MDM2/Lid-short and MDM2/Lid. For the version with lid, two representative "closed and disordered" and "open and ordered" lid conformations were constructed from the free-energy surface depicted in Fig. 3B and previous crystallographic data. The standard free energies of binding computed for the two ligands and the three different MDM2 states are summarised in Fig. 5 (Fig. S9† for detailed convergence profiles).

The calculated binding free energies show that Nutlin-3a binds more favourably to MDM2/Lid-closed than MDM2/Lid-short by *ca.* 1 kcal mol^{-1} (Fig. 5A). This is consistent with the slight preference for MDM2/Lid observed in ITC experiments. Nutlin-3a further shows a *ca.* 0.5 kcal mol^{-1} preference for binding to MDM2/Lid-ordered when compared to MDM2/Lid-closed. In the case of AM-7209 the MDM2/Lid-closed state is the least preferred, followed by MDM2/Lid-short, and MDM2/Lid-ordered. The latter is favoured over MDM2/Lid-closed by *ca.* 3 kcal mol^{-1} and over MDM2/Lid-short by *ca.* 1.5 kcal mol^{-1} (Fig. 5B).

The overall picture that emerges is that the "open and ordered" lid macrostate of MDM2 is barely detectable in apo MDM2 because it is *ca.* 1.5 kcal mol^{-1} less stable than the major "closed and disordered" lid microstate. This corresponds to an "open and ordered" equilibrium population of *ca.* 7%. Upon binding to MDM2 Nutlin-3a shows a slight energetic preference of *ca.* 0.5 kcal mol^{-1} for the "open and ordered" lid macrostate, which is insufficient to populate the ordered state to a significant extent (the equilibrium population of "open and ordered" increases to *ca.* 15%). By contrast the strong (*ca.* 3 kcal mol^{-1}) preference in binding energetics of AM-7209 for the "open and ordered" lid macrostate is sufficient to shift the energetic balance towards significantly populating this macrostate (the equilibrium population of "open and ordered" increases to *ca.* 90%) in the protein–ligand complex (Fig. 6A).
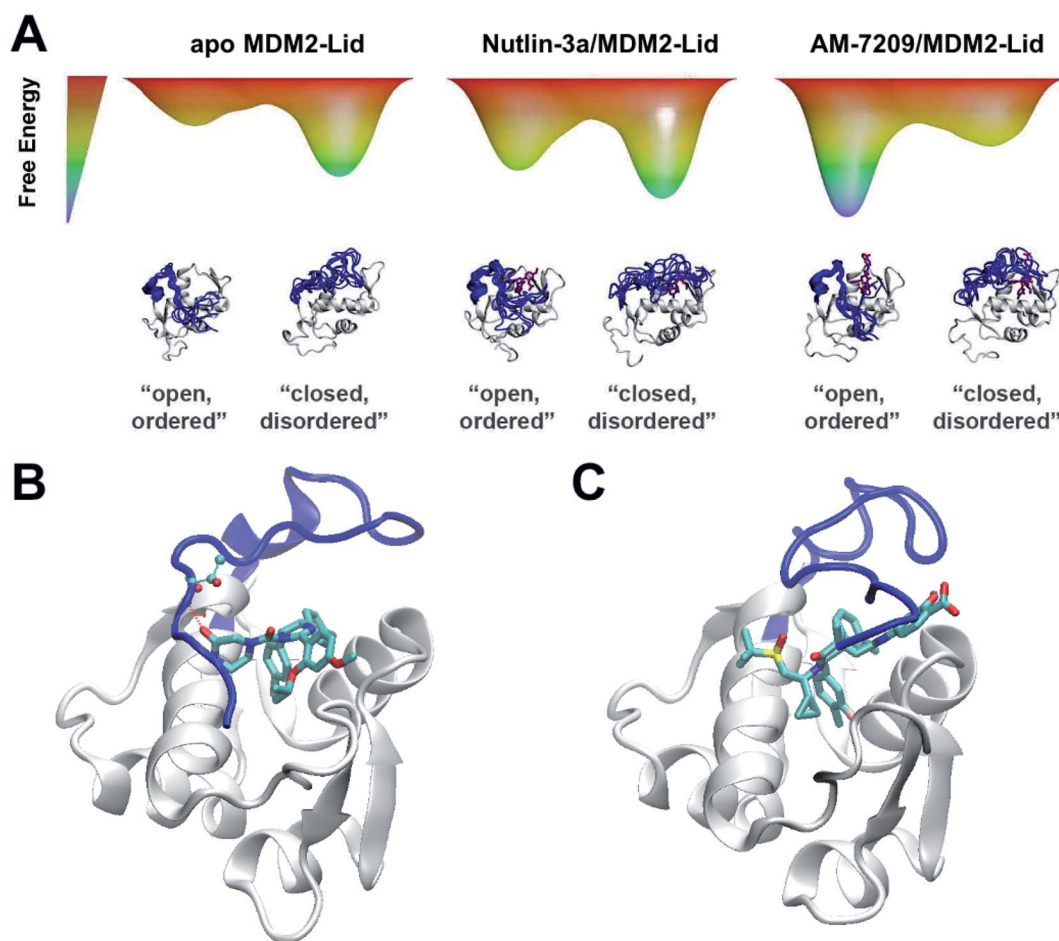

Fig. 6 Mechanistic interpretation of ligand-dependent disorder–order transition of the MDM2 lid IDR. (A) Schematic energy landscapes. (B) Representative snapshot from simulations of MDM2/Lid-closed in complex with Nutlin-3a. (C) Representative snapshot from simulations of MDM2/Lid-closed in complex with AM-7209.

In the case of Nutlin-3a interactions with the lid are stabilising as the calculated free-energy of binding to MDM2/Lid-closed is more negative than to MDM2/Lid-short. For AM-7209 the opposite is observed. This difference is not reproduced when using a docking approach, that favours lid-closed states for both ligands (Fig. S10†). Analysis of the ABFE trajectories suggests that in the "closed and disordered" macrostate the lid lies more frequently above helix α2, and the piperazinone group in Nutlin-3a frequently forms hydrogen-bonding interactions with lid residues and in particular the backbone-NH of Thr10 (Fig. 6B). By contrast, bulkier ring substituents in AM-7209 hinder interactions of lid residues with helix α2 and offer little opportunities for hydrogen-bonding interactions with lid residues (Fig. 6C). In apo MDM2, "closed and disordered" lid conformations remain well hydrated by interfacial water molecules or engage in transient hydrogen bonding interactions with MDM2 core residues. This suggests that energetic preferences for the closed lid state may be tuned by varying the nature of contacts between ligands and lid residues. For instance, in the case of Nutlin-3a replacement of the piperazinone solubilising group by a bulkier and less polar moiety projecting over helix α2 could be pursued to destabilise interactions of the "closed and disordered" lid state with helix α2.

Conclusions

The present study combined calorimetric analysis of protein–ligand interactions with simulations of molecular dynamics to elucidate the energetics of a small molecule-dependent disorder-to-order transition in the oncoprotein MDM2. Our findings provide an explanation for the observation that piperidone ligands order the MDM2 lid IDR.[40] The remarkable 250-fold loss in affinity for AM-7209 arising from truncation of the lid IDR of MDM2 is shown to result from the strong selectivity of this ligand for the "open and ordered" lid macrostate of MDM2 over its "closed and, disordered" microstate. This illustrates the potential value of a ligand-design strategy that seeks to maximise the difference in computed free-energies of binding between ordered and disordered states of an appropriate IDR within the target protein. Such an exercise might be hampered by its demands on computing resources, but the adaptive sampling protocol described here for alchemical absolute calculations of binding free energy affords significant savings in compute time. This should facilitate further investigations of the performances of the diverse forcefields that have been developed to model proteins containing ordered and disordered regions.[59]

More broadly, the present computational strategy, when applied to other IDRs, could benefit future medicinal chemistry programs that target flexible proteins using small molecules.

Methods

Proteins were produced by using pET-20b expression vectors hosted by *Escherichia coli*, C41 or C43 (DE3) cells. Nutlin-3a samples were purchased from APExBio. AM-7209 samples were kindly donated by Amgen. ITC measurements were carried out on a Microcal Auto ITC-200 and the data analysed with MicroCal PEAQ-ITC software version 1.1.0.[60] Accelerated molecular-dynamics and Umbrella sampling simulations were performed using the AMBER16 software suite.[61] Free-energy surfaces were produced with vFEP 0.1.[62] Alchemical free energy calculations were prepared using utilities from the software FESetup,[63] and AMBER16 release, and executed using the SOMD software,[64] as available in Sire release 2019.1 (ref. 65) linked to OpenMM 7.3.1.[66] Detailed experimental and computational protocol details are provided in the ESI.†

Data availability

Input files and code to reproduce the computational results associated with this article are freely available at https://github.com/michellab/MDM2-DG_paper.

Author contributions

C. M. and J. M.: conceptualisation; C. M. and A. A. G.: experimental study; C. M., M. P., S. L. and J. M.: computational study; P. N. B. and J. M.: supervision; C. M. M., M. P., S. L., A. A. G., P. N. B. and J. M.: manuscript preparation.

Conflicts of interest

J. M. is a current member of the Scientific Advisory Board of Cresset.

Acknowledgements

References

1 V. M. Burger, T. Gurry and C. M. Stultz, Intrinsically Disordered Proteins: Where Computation Meets Experiment, *Polymers*, 2014, **6**(10), 2684–2719, DOI: 10.3390/polym6102684.

2 W. Basile, M. Salvatore, C. Bassot and A. Elofsson, Why Do Eukaryotic Proteins Contain More Intrinsically Disordered

Regions?, *PLoS Comput. Biol.*, 2019, **15**(7), 1–20, DOI: 10.1371/journal.pcbi.1007186.

3 P. Santofimia-Castaño, B. Rizzuti, Y. Xia, O. Abian, L. Peng, A. Velázquez-Campoy, J. L. Neira and J. Iovanna, Targeting Intrinsically Disordered Proteins Involved in Cancer, *Cell. Mol. Life Sci.*, 2020, **77**(9), 1695–1707, DOI: 10.1007/s00018-019-03347-3.

4 L. Mollica, L. M. Bessa, X. Hanoulle, M. R. Jensen, M. Blackledge and R. Schneider, Binding Mechanisms of Intrinsically Disordered Proteins: Theory, Simulation, and Experiment, *Front. Mol. Biosci.*, 2016, 52.

5 D. I. Hammoudeh, A. V. Follis, E. V. Prochownik and S. J. Metallo, Multiple Independent Binding Sites for Small-Molecule Inhibitors on the Oncoprotein c-Myc, *J. Am. Chem. Soc.*, 2009, **131**(21), 7390–7401, DOI: 10.1021/ja900616b.

6 B. I. Leach, A. Kuntimaddi, C. R. Schmidt, T. Cierpicki, S. A. Johnson and J. H. Bushweller, Leukemia Fusion Target AF9 Is an Intrinsically Disordered Transcriptional Regulator That Recruits Multiple Partners *via* Coupled Folding and Binding, *Structure*, 2013, **21**(1), 176–183, DOI: 10.1016/J.STR.2012.11.011.

7 J. L. Neira, J. Bintz, M. Arruebo, B. Rizzuti, T. Bonacci, S. Vega, A. Lanas, A. Velázquez-Campoy, J. L. Iovanna and O. Abián, Identification of a Drug Targeting an Intrinsically Disordered Protein Involved in Pancreatic Adenocarcinoma, *Sci. Rep.*, 2017, **7**(1), 39732, DOI: 10.1038/srep39732.

8 J. M. R. Baker, R. P. Hudson, V. Kanelis, W.-Y. Choy, P. H. Thibodeau, P. J. Thomas and J. D. Forman-Kay, CFTR Regulatory Region Interacts with NBD1 Predominantly *via* Multiple Transient Helices, *Nat. Struct. Mol. Biol.*, 2007, **14**(8), 738–745, DOI: 10.1038/nsmb1278.

9 S. Milles, D. Mercadante, I. V. Aramburu, M. R. Jensen, N. Banterle, C. Koehler, S. Tyagi, J. Clarke, S. L. Shammas, M. Blackledge, F. Gräter and E. A. Lemke, Plasticity of an Ultrafast Interaction between Nucleoporins and Nuclear Transport Receptors, *Cell*, 2015, **163**(3), 734–745, DOI: 10.1016/j.cell.2015.09.047.

10 A. Borgia, M. B. Borgia, K. Bugge, V. M. Kissling, P. O. Heidarsson, C. B. Fernandes, A. Sottini, A. Soranno, K. J. Buholzer, D. Nettels, B. B. Kragelund, R. B. Best and B. Schuler, Extreme Disorder in an Ultrahigh-Affinity Protein Complex, *Nature*, 2018, **555**(7694), 61–66, DOI: 10.1038/nature25762.

11 G. Papadakos, A. Sharma, L. E. Lancaster, R. Bowen, R. Kaminska, A. P. Leech, D. Walker, C. Redfield and C. Kleanthous, Consequences of Inducing Intrinsic Disorder in a High-Affinity Protein–Protein Interaction, *J. Am. Chem. Soc.*, 2015, **137**(16), 5252–5255, DOI: 10.1021/ja512607r.

12 J. M. Rogers, C. T. Wong and J. Clarke, Coupled Folding and Binding of the Disordered Protein PUMA Does Not Require Particular Residual Structure, *J. Am. Chem. Soc.*, 2014, **136**(14), 5197–5200, DOI: 10.1021/ja4125065.

13 A. H. S. Martinelli, F. C. Lopes, E. B. O. John, C. R. Carlini and R. Ligabue-Braun, Modulation of Disordered Proteins with a Focus on Neurodegenerative Diseases and Other Pathologies, *Int. J. Mol. Sci.*, 2019, **20**(6), 1322, DOI: 10.3390/ijms20061322.

14 H. Lu, Q. Zhou, J. He, Z. Jiang, C. Peng, R. Tong and J. Shi, Recent Advances in the Development of Protein–Protein Interactions Modulators: Mechanisms and Clinical Trials, *Signal Transduction Targeted Ther.*, 2020, **5**(1), 213, DOI: 10.1038/s41392-020-00315-3.

15 G. T. Heller, F. A. Aprile, T. C. T. Michaels, R. Limbocker, M. Perni, F. S. Ruggeri, B. Mannini, T. Löhr, M. Bonomi, C. Camilloni, A. De Simone, I. C. Felli, R. Pierattelli, T. P. J. Knowles, C. M. Dobson and M. Vendruscolo, Small-Molecule Sequestration of Amyloid-β as a Drug Discovery Strategy for Alzheimer's Disease, *Sci. Adv.*, 2020, **6**(45), eabb5924, DOI: 10.1126/sciadv.abb5924.

16 S. Wallin, Intrinsically Disordered Proteins: Structural and Functional Dynamics, *Res. Rep. Biol.*, 2017, **8**, 7–16, DOI: 10.2147/RRB.S57282.

17 R. Cuchillo and J. Michel, Mechanisms of Small-Molecule Binding to Intrinsically Disordered Proteins, *Biochem. Soc. Trans.*, 2012, **40**(5), 1004–1008, DOI: 10.1042/BST20120086.

18 P. Robustelli, S. Piana and D. E. Shaw, Mechanism of Coupled Folding-upon-Binding of an Intrinsically Disordered Protein, *J. Am. Chem. Soc.*, 2020, **142**(25), 11092–11101, DOI: 10.1021/jacs.0c03217.

19 P. Sormanni, D. Piovesan, G. T. Heller, M. Bonomi, P. Kukic, C. Camilloni, M. Fuxreiter, Z. Dosztanyi, R. V. Pappu, M. M. Babu, S. Longhi, P. Tompa, A. K. Dunker, V. N. Uversky, S. C. E. Tosatto and M. Vendruscolo, Simultaneous Quantification of Protein Order and Disorder, *Nat. Chem. Biol.*, 2017, **13**(4), 339–342, DOI: 10.1038/nchembio.2331.

20 J. Mu, H. Liu, J. Zhang, R. Luo and H.-F. Chen, Recent Force Field Strategies for Intrinsically Disordered Proteins, *J. Chem. Inf. Model.*, 2021, **61**(3), 1037–1047, DOI: 10.1021/acs.jcim.0c01175.

21 O. Abian, S. Vega, J. L. Neira and A. Velazquez-Campoy, Chapter 17 - High-Throughput Screening for Intrinsically Disordered Proteins by Using Biophysical Methods, in *Protein Homeostasis Diseases*, ed. A. L. Pey, Academic Press, 2020, pp. 359–387, DOI: 10.1016/B978-0-12-819132-3.00017-8.

22 J. Michel and R. Cuchillo, The Impact of Small Molecule Binding on the Energy Landscape of the Intrinsically Disordered Protein C-Myc, *PLoS One*, 2012, 7(7), e41070.

23 G. T. Heller, P. Sormanni and M. Vendruscolo, Targeting Disordered Proteins with Small Molecules Using Entropy, *Trends Biochem. Sci.*, 2015, **40**(9), 491–496, DOI: 10.1016/j.tibs.2015.07.004.

24 H. Ruan, Q. Sun, W. Zhang, Y. Liu and L. Lai, Targeting Intrinsically Disordered Proteins at the Edge of Chaos, *Drug Discovery Today*, 2019, **24**(1), 217–227, DOI: 10.1016/j.drudis.2018.09.017.

25 P. Robustelli, S. Piana and D. E. Shaw, Developing a Molecular Dynamics Force Field for Both Folded and Disordered Protein States, *Proc. Natl. Acad. Sci. U. S. A.*, 2018, **115**(21), E4758–E4766, DOI: 10.1073/pnas.1800690115.

26 P. Robustelli, A. Ibanez-de-Opakua, C. Campbell-Bezat, F. Giordanetto, S. Becker, M. Zweckstetter, A. C. Pan and D. E. Shaw, Molecular Basis of Small-Molecule Binding to α-Synuclein, *J. Am. Chem. Soc.*, 2022, **144**(6), 2501–2510, DOI: **10.1021/jacs.1c07591**.

27 S. Nag, J. Qin, K. S. Srivenugopal, M. Wang and R. Zhang, The MDM2-P53 Pathway Revisited, *J. Biomed. Res.*, 2013, **27**(4), 254–271, DOI: **10.7555/JBR.27.20130030**.

28 Ö. Demir, E. P. Barros, T. L. Offutt, M. Rosenfeld and R. E. Amaro, An Integrated View of P53 Dynamics, Function, and Reactivation, *Curr. Opin. Struct. Biol.*, 2021, **67**, 187–194, DOI: **10.1016/j.sbi.2020.11.005**.

29 H.-F. Chen and R. Luo, Binding Induced Folding in P53–MDM2 Complex, *J. Am. Chem. Soc.*, 2007, **129**(10), 2930–2937, DOI: **10.1021/ja0678774**.

30 S. A. Showalter, L. Bruschweiler-Li, E. Johnson, F. Zhang and R. Brüschweiler, Quantitative Lid Dynamics of MDM2 Reveals Differential Ligand Binding Modes of the P53-Binding Cleft, *J. Am. Chem. Soc.*, 2008, **130**(20), 6472–6478, DOI: **10.1021/ja800201j**.

31 J. A. Bueren-Calabuig and J. Michel, Elucidation of Ligand-Dependent Modulation of Disorder-Order Transitions in the Oncoprotein MDM2, *PLoS Comput. Biol.*, 2015, **11**(6), 1–27, DOI: **10.1371/journal.pcbi.1004282**.

32 J. A. Bueren-Calabuig and J. Michel, Impact of Ser17 Phosphorylation on the Conformational Dynamics of the Oncoprotein MDM2, *Biochemistry*, 2016, **55**(17), 2500–2509, DOI: **10.1021/acs.biochem.6b00127**.

33 S. Mukherjee, G. A. Pantelopulos and V. A. Voelz, Markov Models of the Apo-MDM2 Lid Region Reveal Diffuse yet Two-State Binding Dynamics and Receptor Poses for Computational Docking, *Sci. Rep.*, 2016, **6**(1), 31631, DOI: **10.1038/srep31631**.

34 K. Ding, Y. Lu, Z. Nikolovska-Coleska, S. Qiu, Y. Ding, W. Gao, J. Stuckey, K. Krajewski, P. P. Roller, Y. Tomita, D. A. Parrish, J. R. Deschamps and S. Wang, Structure-Based Design of Potent Non-Peptide MDM2 Inhibitors, *J. Am. Chem. Soc.*, 2005, **127**(29), 10130–10131, DOI: **10.1021/ja051147z**.

35 Y. Zhao, L. Liu, W. Sun, J. Lu, D. McEachern, X. Li, S. Yu, D. Bernard, P. Ochsenbein, V. Ferey, J.-C. Carry, J. R. Deschamps, D. Sun and S. Wang, Diastereomeric Spirooxindoles as Highly Potent and Efficacious MDM2 Inhibitors, *J. Am. Chem. Soc.*, 2013, **135**(19), 7223–7234, DOI: **10.1021/ja3125417**.

36 M. J. Hansen, F. M. Feringa, P. Kobauri, W. Szymanski, R. H. Medema and B. L. Feringa, Photoactivation of MDM2 Inhibitors: Controlling Protein–Protein Interaction with Light, *J. Am. Chem. Soc.*, 2018, **140**(41), 13136–13141, DOI: **10.1021/jacs.8b04870**.

37 M. Konopleva, G. Martinelli, N. Daver, C. Papayannidis, A. Wei, B. Higgins, M. Ott, J. Mascarenhas and M. Andreeff, MDM2 Inhibition: An Important Step Forward in Cancer Therapy, *Leukemia*, 2020, **34**(11), 2858–2874, DOI: **10.1038/s41375-020-0949-z**.

38 W. Wang, J.-J. Qin, M. Rajaei, X. Li, X. Yu, C. Hunt and R. Zhang, Targeting MDM2 for Novel Molecular Therapy:

39 Beyond Oncology, *Med. Res. Rev.*, 2020, **40**(3), 856–880, DOI: **10.1002/med.21637**.

39 Y. Rew, D. Sun, X. Yan, H. P. Beck, J. Canon, A. Chen, J. Duquette, J. Eksterowicz, B. M. Fox, J. Fu, A. Z. Gonzalez, J. Houze, X. Huang, M. Jiang, L. Jin, Y. Li, Z. Li, Y. Ling, M.-C. Lo, A. M. Long, L. R. McGee, J. McIntosh, J. D. Oliner, T. Osgood, A. Y. Saiki, P. Shaffer, Y. C. Wang, S. Wortman, P. Yakowec, Q. Ye, D. Yu, X. Zhao, J. Zhou, J. C. Medina and S. H. Olson, Discovery of AM-7209, a Potent and Selective 4-Amidobenzoic Acid Inhibitor of the MDM2–P53 Interaction, *J. Med. Chem.*, 2014, **57**(24), 10499–10511, DOI: **10.1021/jm501550p**.

40 K. Michelsen, J. B. Jordan, J. Lewis, A. M. Long, E. Yang, Y. Rew, J. Zhou, P. Yakowec, P. D. Schnier, X. Huang and L. Poppe, Ordering of the N-Terminus of Human MDM2 by Small Molecule Inhibitors, *J. Am. Chem. Soc.*, 2012, **134**(41), 17059–17067, DOI: **10.1021/ja305839b**.

41 L. T. Vassilev, B. T. Vu, B. Graves, D. Carvajal, F. Podlaski, Z. Filipovic, N. Kong, U. Kammlott, C. Lukacs, C. Klein, N. Fotouhi and E. A. Liu, *In Vivo* Activation of the P53 Pathway by Small-Molecule Antagonists of MDM2, *Science*, 2004, **303**(5659), 844–848, DOI: **10.1126/science.1092472**.

42 D. Song, R. Luo and H.-F. Chen, The IDP-Specific Force Field Ff14IDPSFF Improves the Conformer Sampling of Intrinsically Disordered Proteins, *J. Chem. Inf. Model.*, 2017, **57**(5), 1166–1178, DOI: **10.1021/acs.jcim.7b00135**.

43 P. S. Shabane, S. Izadi and A. V. Onufriev, General Purpose Water Model Can Improve Atomistic Simulations of Intrinsically Disordered Proteins, *J. Chem. Theory Comput.*, 2019, **15**(4), 2620–2634, DOI: **10.1021/acs.jctc.8b01123**.

44 A. K. Somavarapu and K. P. Kepp, The Dependence of Amyloid-β Dynamics on Protein Force Fields and Water Models, *ChemPhysChem*, 2015, **16**(15), 3278–3289, DOI: **10.1002/cphc.201500415**.

45 V. H. Man, X. He, P. Derreumaux, B. Ji, X.-Q. Xie, P. H. Nguyen and J. Wang, Effects of All-Atom Molecular Mechanics Force Fields on Amyloid Peptide Assembly: The Case of Aβ16–22 Dimer, *J. Chem. Theory Comput.*, 2019, **15**(2), 1440–1452, DOI: **10.1021/acs.jctc.8b01107**.

46 V. Zapletal, A. Mládek, K. Melková, P. Louša, E. Nomilner, Z. Jaseňáková, V. Kubáň, M. Makovická, A. Laníková, L. Žídek and J. Hritz, Choice of Force Field for Proteins Containing Structured and Intrinsically Disordered Regions, *Biophys. J.*, 2020, **118**(7), 1621–1633, DOI: **10.1016/j.bpj.2020.02.019**.

47 Y. Gao, C. Zhang, X. Wang and T. Zhu, A Test of AMBER Force Fields in Predicting the Secondary Structure of α-Helical and β-Hairpin Peptides, *Chem. Phys. Lett.*, 2017, **679**, 112–118, DOI: **10.1016/j.cplett.2017.04.074**.

48 Y. Zheng and Q. Cui, The Histone H3 N-Terminal Tail: A Computational Analysis of the Free Energy Landscape and Kinetics, *Phys. Chem. Chem. Phys.*, 2015, **17**(20), 13689–13698, DOI: **10.1039/C5CP01858G**.

49 L. C. T. Pierce, R. Salomon-Ferrer, C. A. F. De Oliveira, J. A. McCammon and R. C. Walker, Routine Access to Millisecond Time Scale Events with Accelerated Molecular

Dynamics, *J. Chem. Theory Comput.*, 2012, **8**(9), 2997–3002, DOI: **10.1021/ct300284c**.

50 G. M. Torrie and J. P. Valleau, Nonphysical Sampling Distributions in Monte Carlo Free-Energy Estimation: Umbrella Sampling, *J. Comput. Phys.*, 1977, **23**(2), 187–199, DOI: **10.1016/0021-9991(77)90121-8**.

51 T.-S. Lee, B. K. Radak, M. Huang, K.-Y. Wong and D. M. York, Roadmaps through Free Energy Landscapes Calculated Using the Multidimensional VFEP Approach, *J. Chem. Theory Comput.*, 2014, **10**(1), 24–34, DOI: **10.1021/ct400691f**.

52 W. L. Jorgensen, J. K. Buckner, S. Boudon and J. Tirado-Rives, Efficient Computation of Absolute Free Energies of Binding by Computer Simulations. Application to the Methane Dimer in Water, *J. Chem. Phys.*, 1988, **89**(6), 3742–3746, DOI: **10.1063/1.454895**.

53 M. K. Gilson, J. A. Given, B. L. Bush and J. A. McCammon, The Statistical-Thermodynamic Basis for Computation of Binding Affinities: A Critical Review, *Biophys. J.*, 1997, **72**(3), 1047–1069, DOI: **10.1016/S0006-3495(97)78756-3**.

54 M. Aldeghi, A. Heifetz, M. J. Bodkin, S. Knapp and P. C. Biggin, Predictions of Ligand Selectivity from Absolute Binding Free Energy Calculations, *J. Am. Chem. Soc.*, 2017, **139**(2), 946–957, DOI: **10.1021/jacs.6b11467**.

55 M. Aldeghi, A. Heifetz, M. J. Bodkin, S. Knapp and P. C. Biggin, Accurate Calculation of the Absolute Free Energy of Binding for Drug Molecules, *Chem. Sci.*, 2016, **7**(1), 207–218, DOI: **10.1039/C5SC02678D**.

56 A. S. J. S. Mey, B. K. Allen, H. E. B. Macdonald, J. D. Chodera, D. F. Hahn, M. Kuhn, J. Michel, D. L. Mobley, L. N. Naden, S. Prasad, A. Rizzi, J. Scheen, M. R. Shirts, G. Tresadern and H. Xu, Best Practices for Alchemical Free Energy Calculations [Article v1.0], *Living J. Comput. Mol. Sci.*, 2020, **2**(1), 18378, DOI: **10.33011/livecoms.2.1.18378**.

57 Z. Cournia, B. K. Allen, T. Beuming, D. A. Pearlman, B. K. Radak and W. Sherman, Rigorous Free Energy Simulations in Virtual Screening, *J. Chem. Inf. Model.*, 2020, **60**(9), 4153–4169, DOI: **10.1021/acs.jcim.0c00116**.

58 M. R. Shirts and J. D. Chodera, Statistically Optimal Analysis of Samples from Multiple Equilibrium States, *J. Chem. Phys.*, 2008, **129**(12), 124105, DOI: **10.1063/1.2978177**.

59 A. Kuzmanic, R. B. Pritchard, D. F. Hansen and F. L. Gervasio, Importance of the Force Field Choice in Capturing Functionally Relevant Dynamics in the von Willebrand Factor, *J. Phys. Chem. Lett.*, 2019, **10**(8), 1928–1934, DOI: **10.1021/acs.jpclett.9b00517**.

60 Malvern Inc., *MicroCal PEAQ-ITC 1.1.0*.

61 D. A. Case, R. M. Betz, D. S. Cerutti, T. E. Cheatham III, T. A. Darden, R. E. Duke, T. J. Giese, H. Gohlke, A. W. Goetz, N. Homeyer, S. Izadi, P. Janowski, J. Kaus, A. Kovalenko, T. S. Lee, S. LeGrand, P. Li, C. Lin, T. Luchko, R. Luo, B. Madej, D. Mermelstein, K. M. Merz, G. Monard, H. Nguyen, H. T. Nguyen, I. Omelyan, A. Onufriev, D. R. Roe, A. Roitberg, C. Sagui, C. L. Simmerling, W. M. Botello-Smith, J. Swails, R. C. Walker, J. Wang, R. M. Wolf, X. Wu, L. Xiao and P. A. Kollman, *Amber 16*, University of California, San Francisco, 2016, DOI: **10.1002/jcc.23031**.

62 T.-S. Lee, B. K. Radak, A. Pabis and D. M. York, A New Maximum Likelihood Approach for Free Energy Profile Construction from Molecular Simulations, *J. Chem. Theory Comput.*, 2013, **9**(1), 153–164, DOI: **10.1021/ct300703z**.

63 H. H. Loeffler, J. Michel and C. Woods, FESetup: Automating Setup for Alchemical Free Energy Simulations, *J. Chem. Inf. Model.*, 2015, **55**(12), 2485–2490, DOI: **10.1021/acs.jcim.5b00368**.

64 G. Calabrò, C. J. Woods, F. Powlesland, A. S. J. S. Mey, A. J. Mulholland and J. Michel, Elucidation of Nonadditive Effects in Protein–Ligand Binding Energies: Thrombin as a Case Study, *J. Phys. Chem. B*, 2016, **120**(24), 5340–5350, DOI: **10.1021/acs.jpcb.6b03296**.

65 C. Woods, A. S. J. S. Mey G. Calabrò and J. Michel, *Sire Molecular Simulation Framework*, 2019.

66 P. Eastman, J. Swails, J. D. Chodera, R. T. McGibbon, Y. Zhao, K. A. Beauchamp, L.-P. Wang, A. C. Simmonett, M. P. Harrigan, C. D. Stern, R. P. Wiewiora, B. R. Brooks and V. S. Pande, OpenMM 7: Rapid Development of High Performance Algorithms for Molecular Dynamics, *PLoS Comput. Biol.*, 2017, **13**(7), e1005659.